BULLETIN OF THE EARTHQUAKE
RESEARCH INSTITUTE
UNIVERSITY OF TOKYO
Vol. 61 (1986) pp. 67-95

The Effect of Asymmetric Insular Shelf in Trapping Long Gravity Waves around an Island

Michiaki HASHIMOTO*
Earthquake Research Institute
(Received January 31, 1986)

Abstract

The effect of asymmetric insular shelf in trapping long gravity waves around an island is investigated numerically by using a simple model. The model consists of a steep-sided, circular island which rises from the top of a circular sill of larger radius. The center of the island is placed off-center of the sill by Δr distance.

The results are: (1) As the asymmetry becomes pronounced, the region of higher amplitude response shifts to the direction of the broader shelf. (2) The transfer function in the case of an asymmetric island can be estimated roughly by using the solution of a symmetric island model whose width of the round shelf coincides with the broadest width of the shelf in the asymmetric model.

In water level observations at four stations around Oshima Island, a spectrum peak of period approximately 8 minutes could often be detected at the westernmost station. To understand this feature, numerical calculations were made both for the realistic Oshima-Island model (with actual bathymetry), and for the Island-Shelf model (which roughly approximated the topography of the Oshima Island area). And it was found that the oscillations of the observed peak period of 8 min. corresponded to a (1, 0) mode of edge wave. This mode is modified by the asymmetry of the insular shelf and forms a standing wave pattern with a node extending in the southwesterly direction vis-a-vis Oshima Island.

1. Introduction

Trapping problems of long gravity waves around an island have been studied for a long time. It is the extention of the edge wave idea to the topography with concentric circular contours.

In the case of an island, unlike a straight coast, perfect trapping no longer occurs for the free wave motion, and wave energy is scattered

* Present address: Japan Weather Association, 2-9-2 Kanda Nishikimachi, Chiyoda-ku Tokyo, Japan.

away from the guiding bathymetric contour if the depth of water is finite at a great distance. Physically because the waves which propagate from the inside of concentric circular region to the outside are not reflected back completely unless the depth of water increases more than r^2 at $r \to \infty$. Mathematically it corresponds to the fact that the eigen frequency inevitably has an imaginary part. But if this imaginary part is extremely small, we may say that the wave is practically trapped. Thus, if the incident wavetrain is well tuned, the energy is trapped effectively around an island and a large response is expected near the shoreline. In this sense, we can regard an island as a resonator of long waves with particular frequencies.

LONGUET-HIGGINS (1967) first studied this problem. He considered wave motion above a stepped circular sill within the framework of shallow water theory and showed the existence of eigen frequencies with extremely small imaginary parts. So, a train of plane waves with a frequency near such an eigen frequency can excite "nearly trapped modes" over the sill. In his model, the largest responses occur at the higher angular modes and at smaller ratio of the depths of the sill and open ocean.

SUMMERFIELD (1972) considered a model consisting of a cylindrical island rising from the top of a round sill of larger radius. He showed the eigen frequencies for his system to be closely related to those of the LONGUET-HIGGINS model.

On the other hand, RENARDY (1983) has examined the validity of long wave approximation in the model of LONGUET-HIGGINS. Her study was motivated by the fact that the large responses predicted by the theory were not well borne out by the experiments of BARNARD, PRITCHARD and PROVIS (1983).

In general, if the depth of water is a function of only a distance from the center of an island, the long wave equation splits into a pair of ordinary differential equations, but a symmetric island is seldom found in the real ocean, and in many cases both the shape and the bottom topography around islands are asymmetric. Therefore, it is interesting to investigate the effect caused by asymmetry in trapping wave energy, and, in the present study, we examined the effect of asymmetry in the width of insular shelf by means of numerical simulation. Furthermore, we observed water level oscillations around Oshima Island and interpreted those data in the light of the results obtained by the numerical study.

2. Response analysis by Island-Shelf model

2.1. Fundamental equations

Let x, y be horizontal cartesian coordinate directed to the east and north respectively and z the vertical coordinate directed upward with the origin at the undisturbed sea surface. Then, the linearized, depth-integrated shallow water equations of motion and continuity can be written as

$$\frac{\partial Q_x}{\partial t}=-gh\frac{\partial \eta}{\partial x} \tag{1}$$

$$\frac{\partial Q_y}{\partial t}=-gh\frac{\partial \eta}{\partial y} \tag{2}$$

and

$$\frac{\partial \eta}{\partial t}=-\left(\frac{\partial Q_x}{\partial x}+\frac{\partial Q_y}{\partial y}\right) \tag{3}$$

where Q_x and Q_y are the depth-integrated transport components in the direction of x and y respectively, η is the elevation of the free surface above its equilibrium level, h is the depth of the sea and g the acceleration of gravity.

In the above formulation, the Coriolis force is neglected because the period of waves considered here is much less than the inertial period. Further the frictional forces are also neglected so that the obtained response may be somewhat overestimated. For the wave motion of a shorter period and horizontally smaller scale, we must take the limitation of long wave approximation into account.

Using rectangular grids with spacing Δs and replacing (1), (2) and (3) by a finite difference scheme, the spatial distribution of η, Q_x and Q_y can be computed with time increment Δt. We use an explicit, space-staggered scheme and leap-frog method in time.

To determine the response of the system, we give continual forcing to the system. Taking $r(t)$ as the impulse response function of the island, the response $f_0(t)$ to the input time series $f_i(t)$ can be expressed as follows.

$$f_0(t)=\int_{-\infty}^{\infty} f_i(t')r(t-t')dt'. \tag{4}$$

Taking Fourier transform of both sides, we obtain

$$F_0(\omega)=F_i(\omega)\cdot R(\omega) \tag{5}$$

where F_0, F_i and R are the Fourier transforms of f_0, f_i and r respectively,

and ω is the angular frequency. We can understand the system characteristics by determining $R(\omega)$ at each grid point in space.

When the island has a symmetric insular shelf, waves with certain frequencies are effectively trapped, and $R(\omega)$ has sharp peaks at these frequencies. In the following, we use a simple model representing an asymmetric island and examine how $R(\omega)$ changes as the asymmetry of the insular shelf becomes pronounced.

2.2. Initial and boundary conditions

A plane wave of the Gaussian type is given initialy and propagated freely in the y-direction obeying equations (1)~(3).

The elevation of frequency-band-limited, initial incident wave, H_{ij}, is defined by the Fourier Series

$$H_{ij}=\sum_{l=0}^{M} a_0 e^{-9/2l^2}\cos\left[2\pi l\cdot\frac{\Delta s}{\Delta t\sqrt{gh}}\cdot(j-js)/NT\right] \qquad (6)$$

where (i, j) means grid points, $l=\omega/\Delta\omega$ is integer, NT is the maximum number of time intervals, M is the maximum number of frequency intervals and js is a constant determining initial y-coordinate of the pulse peak. The initial plane wave profile used in the Island-Shelf model has a 6.3 km half-amplitude-width along y-coordinate with a 2.0 m peak amplitude.

The coast is assumed to be rigid vertical walls with perfect reflection. An approximate boundary condition is applied on open boundaries to allow waves to escape from the region concerned. For example, along a boundary parallel to x-axis, Q_y is computed by

$$Q_y=\pm(gh\eta^2-Q_x^2)^{1/2} \qquad (7)$$

where the sign of Q_x is selected so that the water flows out from the region of calculations when η is positive.

2.3. Island-Shelf model

We consider a cylindrical island of radius r_1 surrounded by the circular sill of larger radius r_2 and depth h_1, beyond which deep water of depth h_2 extends. The center of the island shifts by Δr from that of the insular shelf (see Fig. 1). Thus this model represents the asymmetry of the insular shelf. In the real scale we settled the depth of ocean at 4500 m, the depth of the shelf at 500 m, the radius of the sill at 30 km and the radius of the island at 10 km. The domain of calculation is $160\times 250\,\mathrm{km}^2$ and the grid interval Δs is 1 km. Taking the stability condition of numerical calculation into account, Δt is chosen to be 1.5 second. The outer ocean used in this model is a channel with reflecting boundaries

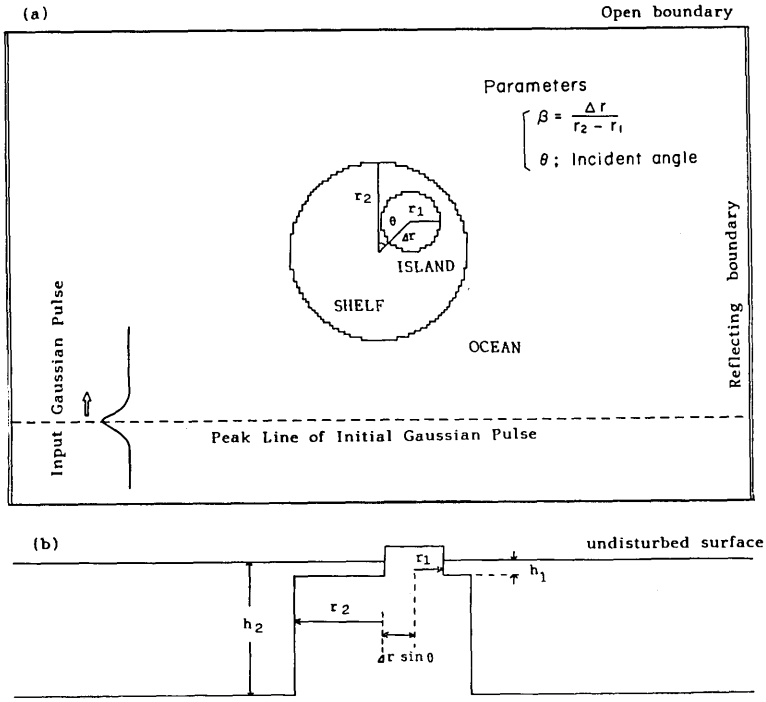

Fig. 1. Island-Shelf model; (a) plan view (b) radial cross-section.

parallel to the propagation direction (the y-axis) of the incident wave and open boundaries normal for it.

We made the experiments changing the incident angle in five ways every 45° from 0° to 180° by rotating the island relative to the propagation direction. We also changed the distance Δr every 2km from the symmetric case (i. e. $\Delta r=0$) to the case in which the edge of the island reaches that of the shelf (i. e. $\Delta r=r_2-r_1$).

Now define the asymmetry parameter β as follows.

$$\beta=\Delta r/(r_2-r_1) \tag{8}$$

That is, $\beta=0$ when the insular shelf is symmetric, $\beta=1$ when the edge of the island reaches that of the sill.

2.4. Verification of the numerical calculation

To simulate the wave response, the following numerical procedure was used. (1) let the initial Gaussian wave propagating freely over the region concerned and record the water elevation until the output spectrum becomes almost steady, (2) make the Fourier analysis upon the time history of the water elevation for each shoreline grid point, (3) establish

a system function as the ratio of the spectrum of output to that of input, and (4) average the system functions around the island and establish the transfer function.

In order to secure the proper numerical input spectrum, the water elevation recorded at the center of a constant depth model (4500m) with the same parameters, dimensions, and input as the Island-Shelf model was calculated by the Fourier analysis. The parameters of H_{ij} in (4) were $M=410$, $NT=10240$, $js=133$ and 512 records with an interval of 30 sec were used in the Fourier analysis by FFT method. As shown in Fig. 2, the numerical input spectrum obtained this way agrees with the analytic one. In the figure, ν is the nondimensional frequency corresponding to the frequency ω, and is defined by

$$\nu=\omega r_2/\sqrt{gh_1}. \tag{9}$$

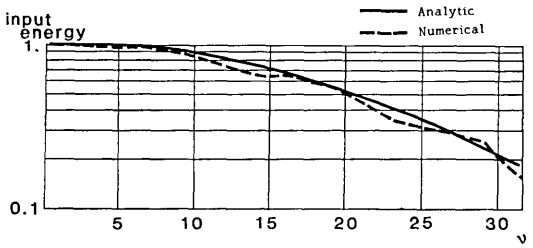

Fig. 2. Comparison of numerical and analytic input spectra.

At first, for the island with a symmetric shelf, the numerical results were compared with the analytical solution to examine the accuracy of the numerical computation.

The result of comparison between numerical transfer function and the analytic solution is shown in Fig. 3-(a). It reveals fairly good agreement between them for frequencies of $\nu=14$ and less. At periods below 3.2 min ($\nu>14$), a shift from the analytic solution develops in the numerical result that may be caused by the use of rectangular grid approximation instead of true circular bathymetric contours. But the shift of the peak frequency at $\nu\sim10$ is less than one grid size reestimated in the space coordinate. And the long wave approximation is satisfied at $\nu\sim10$ with less than 7% error. Further, if it is assumed that ten grids are necessary to describe a wave, then the highest nondimensional frequency to describe a wave at the shallowest depth would be $\nu=19$.

Fig. 3-(b) illustrates the analytical transfer function classified into various azimuthal modes. From now on, we will take n to mean the number of angular nodes and m the number of radial nodes. For example, at the peak of $\nu=3.2616$, $(n, m)=(1, 0)$ mode is dominant and the

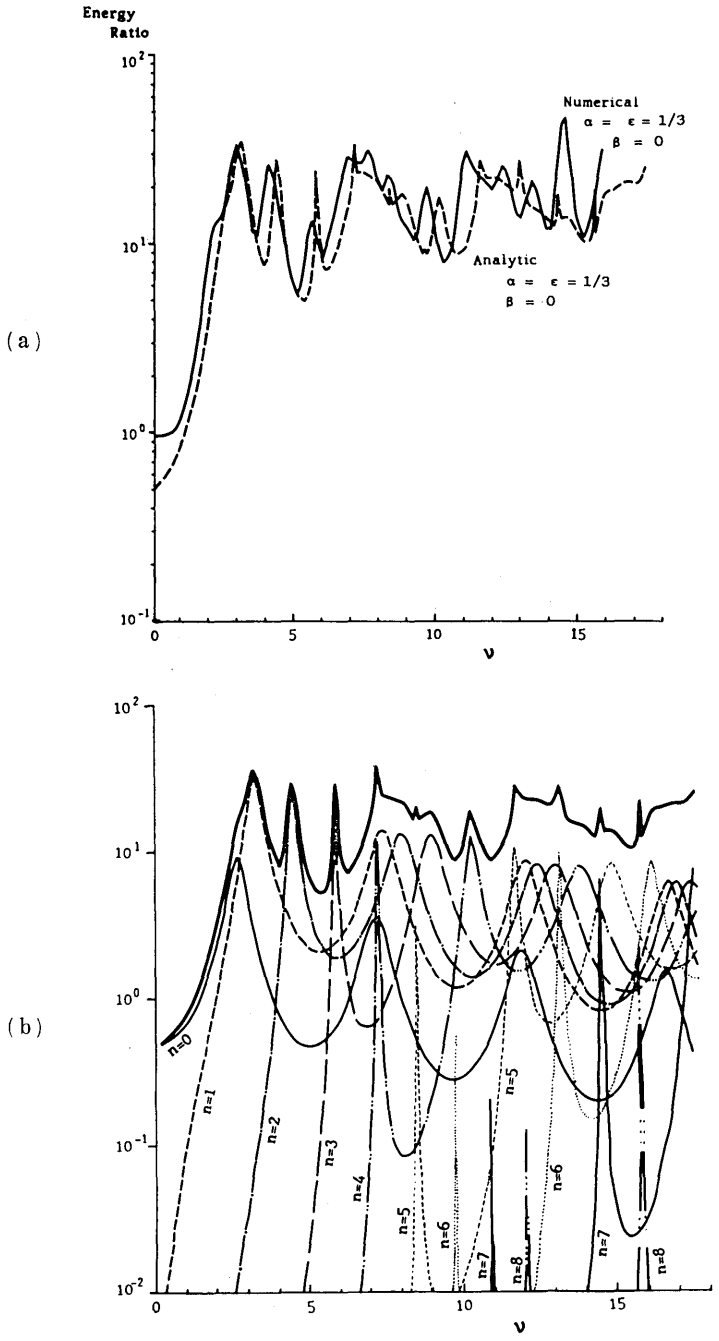

Fig. 3. (a) Comparison of numerical (solid line) and analytic (broken line) transfer function for a symmetric island. Nondimensional parameters are defined by $\alpha=r_1/r_2$, $\varepsilon=(h_1/h_2)^{1/2}$ and $\beta=\Delta r/(r_2-r_1)$. (b) Analytic transfer function classified into various angular modes. Thick line shows the analytic transfer function, and n denotes the number of angular nodes.

shoreline amplitude (square root of energy ratio) is amplified about six times. Similarly $(n, m)=(2, 0)$ mode is dominant at $\nu=4.4880$. However, in higher frequencies we cannot tell which mode contributes most to the

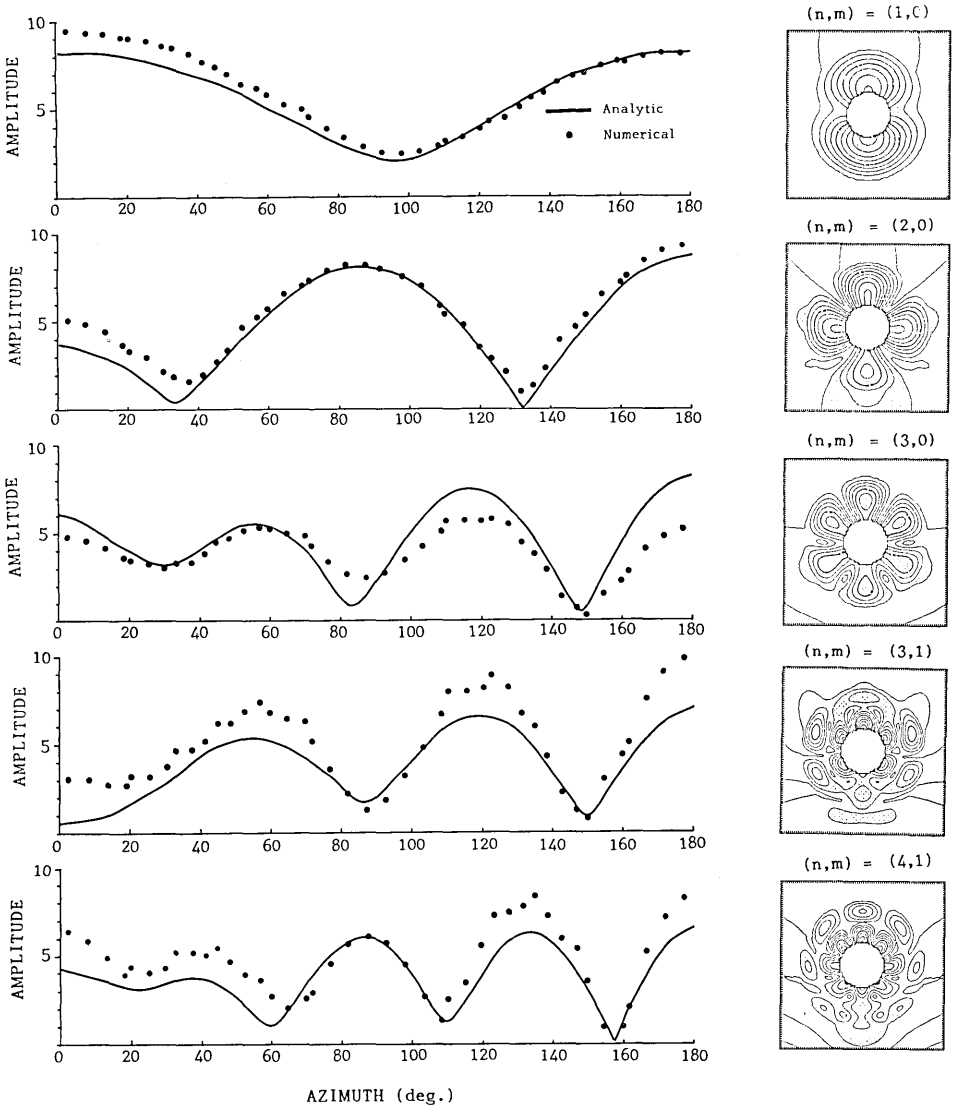

Fig. 4. Comparison of a numerical model with the analytic solution for typical response patterns. The incident side of the island is 0°. Shape parameters are fixed at $\alpha=\varepsilon=1/3$ and $\beta=0.0$. n denotes the number of characteristic angular nodes, and m denotes the number of characteristic radial nodes. The nondimensional frequency of the analytic solution is ν_A and the numerical one is ν_N, and from the top of the figure, each value (ν_A, ν_N) is; (3.26, 3.16), (4.49, 4.21), (5.89, 5.79), (8.91, 8.42), (10.24, 9.82) respectively.

transfer function because higher modes in both radial and azimuthal direction are superposed in a complex manner.

For typical response patterns, the maximum amplitude of waves given by the numerical computations versus azimuth is plotted in Fig. 4, and is compared with the analytical solution of amplitudes on the shoreline. In this figure the azimuth exposed to the incident wave is 0°. Fairly good agreement is found for lower modes, and the expected mode contribution is also represented in the horizontal distribution pattern around the island. From these comparisons, we may say the numerical results are reliable at nondimensional frequencies below 10.

2.5. Results of response analysis

In order to determine the response behavior for each shoreline point, contours of amplification factor versus frequencies were plotted on a perimeter diagram. The result is illustrated in Fig. 5.

In the symmetric case ($\beta=0$), a highly amplified pattern around the island can be found at several discrete frequencies. The corresponding frequencies of large amplification and the peak frequencies in Fig. 3-(a) correspond to each other. But when β increases and the asymmetry of insular shelf becomes pronounced, the region of large amplification becomes limited in the direction of the broader shelf for any incident angle, and also it is observed that the peak frequency which corresponds to the lowest mode shifts to a longer period. If we broaden the shelf width for the symmetric island (that is to say, if the ratio r_1/r_2 becomes small), an analytical solution will show the same tendency in that its peak frequency will also shift to a longer period. So in the case of incident angle 0°, we compare the numerical transfer function with the analytic one which is obtained by changing the symmetric shelf width to the broadest width for each β. The solid lines of Fig. 6 show the numerical solutions in the asymmetric case, and the dashed lines show the analytical solutions with converted shelf width. From this figure, the peak frequencies and energy levels are found to be in fairly good agreement for each β. Therefore, we can surmise an averaged amplification factor in the asymmetric case by using the analytical solution of the symmetric model (which has a uniform shelf width equal to that of the broadest shelf width in the asymmetric model).

Fig. 7-(a)$\sim$(c) illustrates a transition (according to the value of β) of the horizontal distribution pattern around the island for the simpler modes ($(n, m)\sim(0, 0)$, $(1, 0)$, $(2, 0)$). Fig. 7-(a) shows the pattern in which $(0, 0)$ and $(1, 0)$ modes contribute equally when the insular shelf is symmetric. When $\beta=0$ a large response occurs on the lee side of the island because both modes are in phase there. But as β increases and asym-

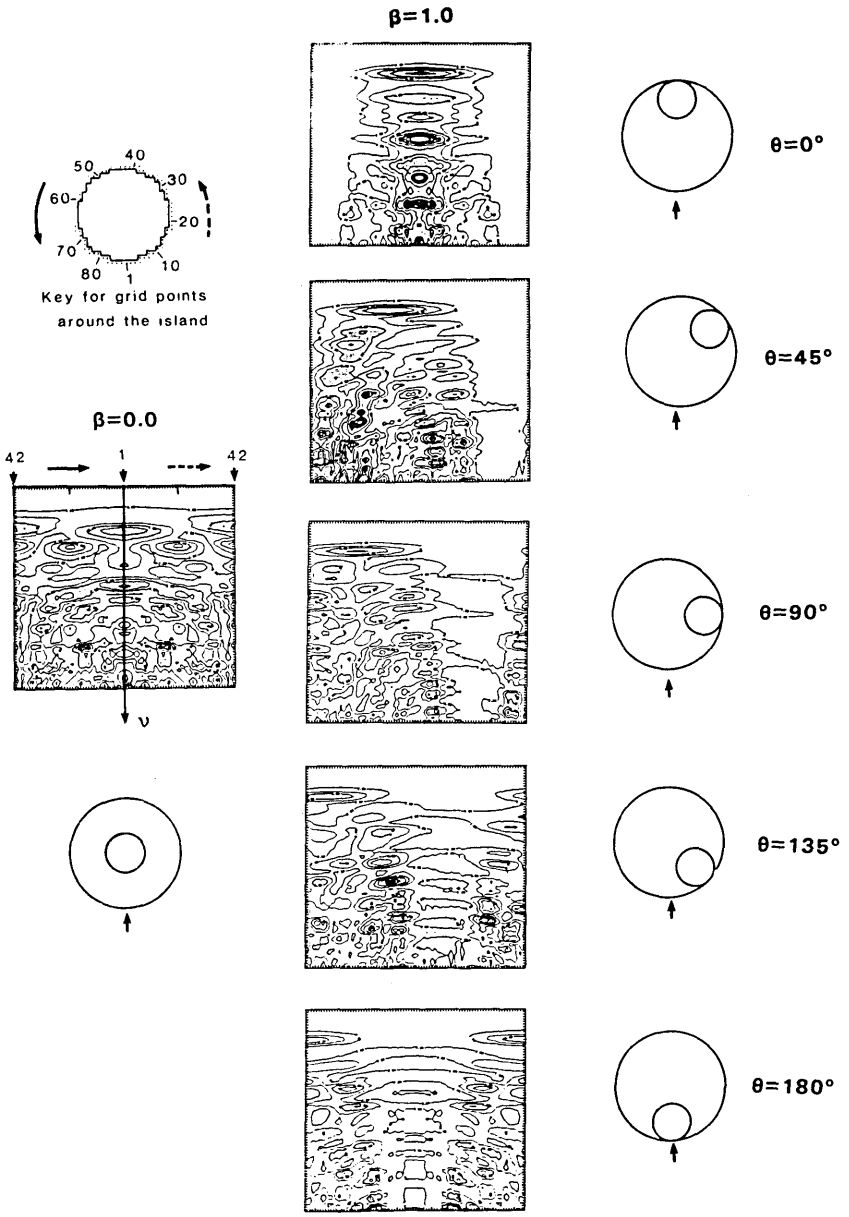

Fig. 5. Contour of the amplification factor around the island. For each incident angle the perimeter is numbered counterclockwise starting with the nearest point to the incident direction. The numbering system places the incident side at the center of the contour map. ν is the nondimensional frequency and ranges from 0 to 15 in equal increments.

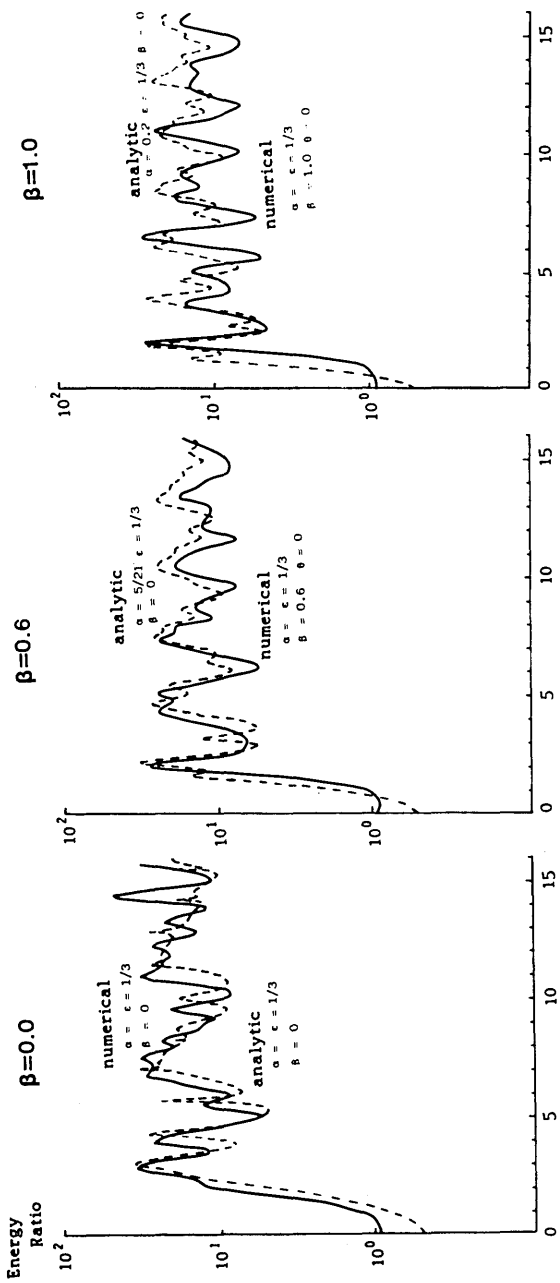

Fig. 6. Comparison of numerical transfer function with analytic solution obtained by changing the width of the symmetric shelf to the broadest one of asymmetric shelf. Solid line shows numerical transfer function and dashed line shows analytic solution with the converted insular shelf. Incident angle is $\theta=0°$.

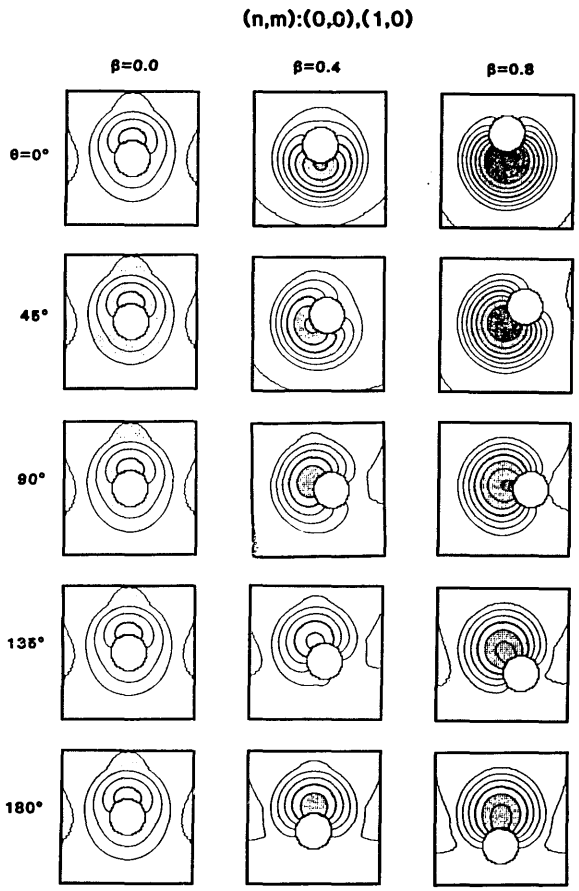

Fig. 7. (a)

metry is pronounced, the location of a large response shifts to the area of broader shelf for any incident direction. This tendency was found even for $\beta=0.2$ although it is not shown in the figure. Fig. 7-(b) shows a case in which the (1, 0) mode is dominant. In the case of incident angle 0° or 180°, tracing the movement of the spatial pattern of this mode becomes difficult, but at other incident angles, it can be seen that a large response region shifts to the direction of a broader shelf. Furthermore, a similar tendency can be seen for the (2, 0) mode (see Fig. 7-(c)). However, for this mode, its pattern in the symmetric case is maintained relatively well at incident angle 45°, 135°. This is because the island moves in the direction where the response is relatively small when $\beta=0$.

Thus, as the asymmetry becomes pronounced, a large response region shifts in the direction of the broader shelf as a whole. Nevertheless, examining the phenomena in more detail, it is found that both the

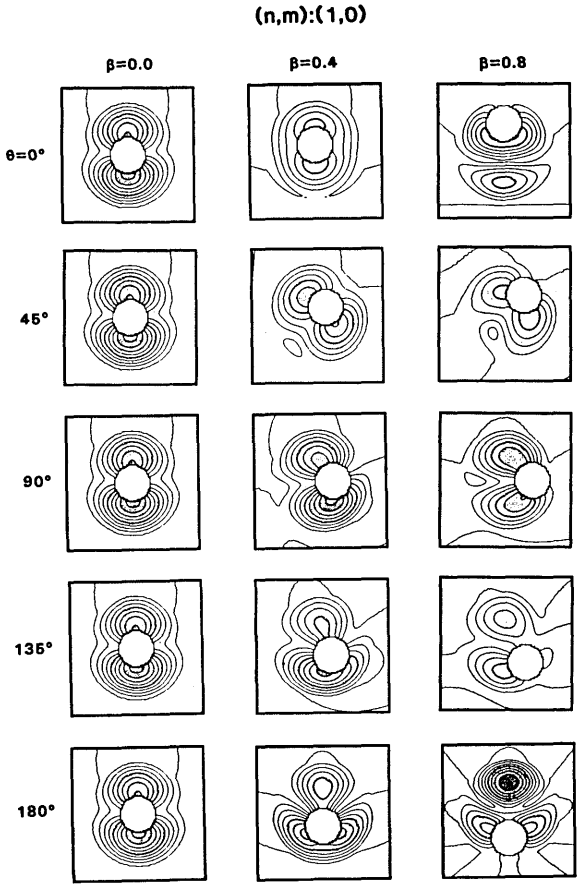

Fig. 7. (b)

characteristic frequency and its energy level differ subtly for the different modes and incident angles (see Fig. 8). For example, the relative power for (1, 0) and (2, 0) modes at $\beta=1.0$ decreases to 30~50 percent of the level in the symmetric case. On the contrary, the power contribution of the (0, 0) mode wave increases especially at 0° and 45°. Moreover, the characteristic frequency for the (1, 0) mode becomes higher as β increases, while the opposite is found to be true in the case of the (0, 0) mode.

Therefore when many modes overlap, the total energy level (summed up to the frequency $\nu=14$) at the shoreline depends very significantly on the incident wave direction (see Fig. 9-(a)). At $\theta=0°$, as asymmetry becomes pronounced, the energy level decreases almost uniformly, and finally decreases to approximately 70 percent of the symmetric case at $\beta=1.0$. On the other hand, at $\theta=45°$ and $\beta=0.8$, the relative energy level increases and reaches a peak at a level approximately 20 percent

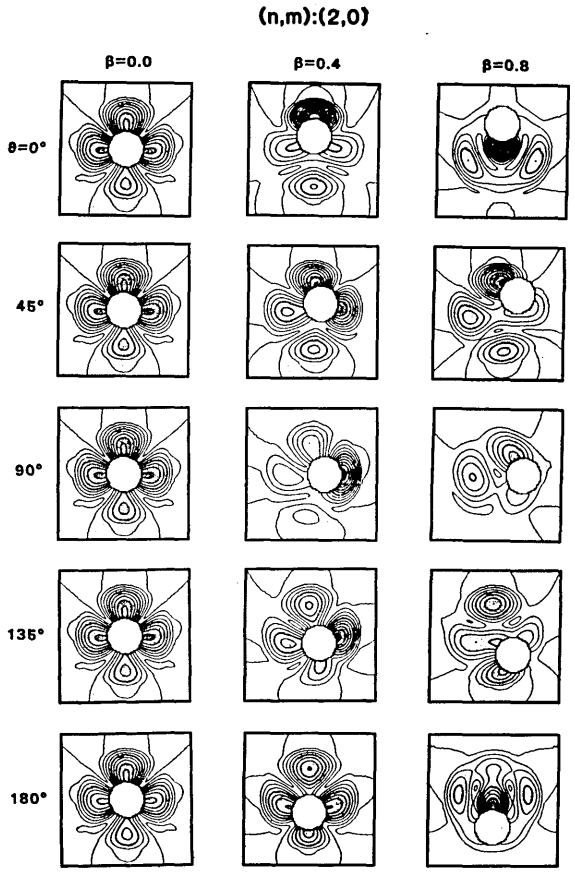

Fig. 7. (c)

Fig. 7. Transition of horizontal distribution pattern for typical modes; (a) (n, m); (0, 0), (1, 0) (b) (n, m); (1, 0) (c) (n, m); (2, 0). For the same incident direction (θ), asymmetry of insular shelf (β) becomes pronounced to the right of each row. Incident waves approach from lower side of each figure. Note that results of $\beta=0.0$ show the same pattern for all θ.

higher than the level reached in the case of symmetric model. For other incident angles, there exists a parameter range in which the relative energy level is unaffected by asymmetry. According to the calculations of total energy levels above the shelf, each specific case has a maximum at some value of β except for $\theta=0°$ (see Fig. 9-(b)).

From these analyses, it is doubtful if the idea of mode decomposition can be applied in the asymmetric case to estimate the total energy level. Even if it could adequately be applied, we would not be able to trace the change of each mode separately. Moreover, since the response apparently depends on both the radius ratio r_1/r_2 and the depth ratio

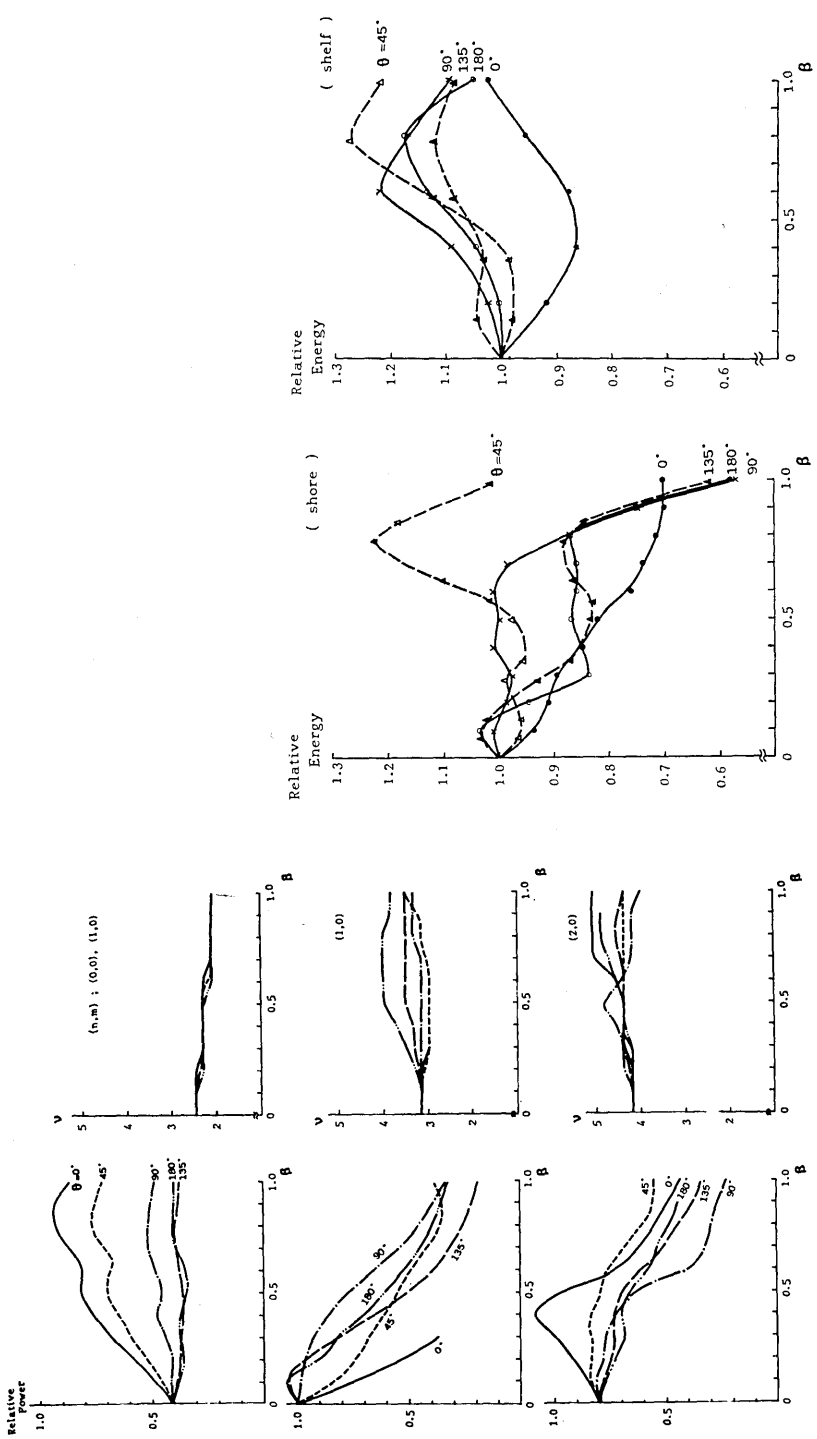

Fig. 8. Relative energy level and frequency corresponding to the characteristic spatial pattern as a function of β: (n, m) denotes a pair of characteristic modes and θ denotes the incident angle. Energy level is normalized by that of the symmetric (1, 0) mode.

Fig. 9. Relative total energy level as a function of asymmetry parameter β for each incident direction; (a) at the shore, (b) above the shelf. The ordinate shows the total energy level at the nondimensional frequencies below 14, normalized by that of the symmetric case (β=0.).

h_1/h_2, it is extremely difficult to understand quantitatively the change of transfer function as a function of various parameters without resort to numerical results.

3. Response analysis for Oshima Island

3.1. Observation of water levels around Oshima Island

We chose Oshima Island as a model to examine the results of the Island-Shelf model in a real ocean for three reasons. (1) Oshima Island is an isolated island facing the open sea, its shape is close to circular and relatively simple. (2) The shoal is spread on the west side of the island and the bottom topography is remarkably asymmetric. (3) Water level records are obtained continuously at the Senzu Tsunami Observatory, located on the northeastern side of the island.

We made simultaneous observations of water levels at four stations shown in Fig. 10 from 18 to 26 November 1983 and the following results were obtained (HASHIMOTO *et al.* 1986). (1) The total amplitude is about 1.0～1.5 cm at Senzu and Komatsubayashi located on the northeastern and eastern coast of Oshima Island respectively, in contrast to about 2.5 cm at Sashikiji and Nomashi located on the southern and western coast respectively (see Fig. 11). (2) A spectrum peak at a period of approximately 8 minutes can often be detected at Nomashi, but characteristic peaks rarely appear at Senzu and Komatsubayashi. And at periods

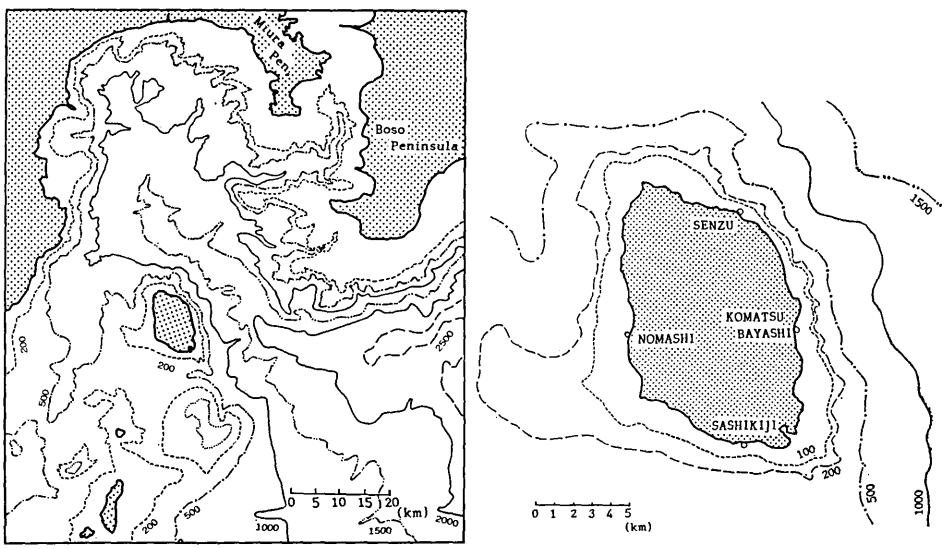

(a) (b)

Fig. 10. (a) A bathymetric map near Izu-Oshima. (b) Observation stations.

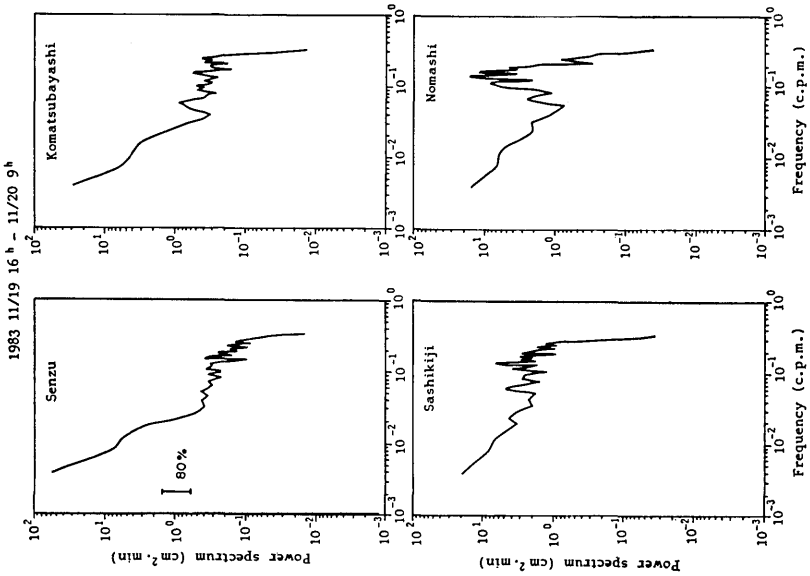

Fig. 12. Power spectrum on 20 November 1983 at each station.

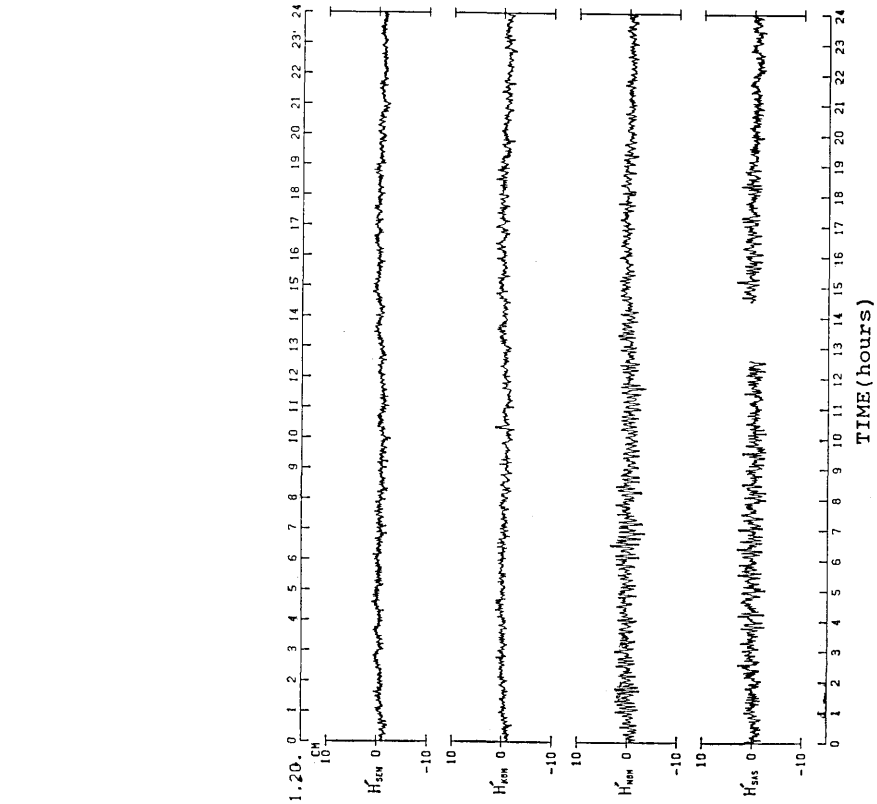

Fig. 11. Band-pass filtered water level records at each station on 20 November 1983. H'_{SEN}, H'_{KOM}, H'_{NOM} and H'_{SAS} means the record of Senzu, Komatsubayashi, Nomashi and Sashikiji respectively. Those records are obtained through band-pass filter with periods ranging from 3 min to 60 min.

shorter than 10 min, the power level is higher at Sashikiji and Nomashi than at Senzu and Komatsubayashi (see Fig. 12).

3.2. Numerical model of Oshima Island

Taking the realistic bottom topography into account, the numerical computation was performed in the domain shown in Fig. 13. The grid interval Δs is taken as 1 km in region I, and 500m in region II in order to calculate the wave forms accurately. η, Q_x and Q_y are linearly interpolated at the junction of two different grid intervals (see AIDA, 1974). Region I is surrounded with open boundaries and we allow waves to escape from this region without reflection.

Following the procedure described in section **2.4**, a time sequence input of Gaussian pulse type with peak amplitude 26.9 cm ($M=200$, $NT=12800$ in (6)) was time-stepped into the Oshima-Island model. We considered four different incident directions, namely east, west, south and north (normal to surrounding boundaries in region I). Taking the stability condition of numerical calculation into account, Δt is chosen to be 1.2 sec.

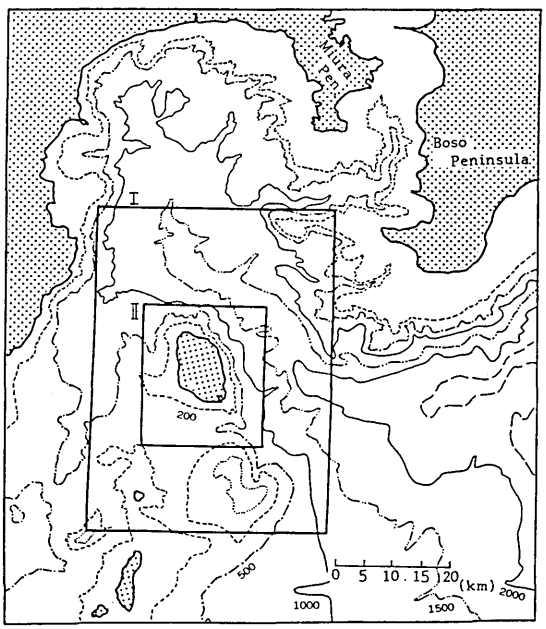

Fig. 13. Computing area of Oshima model. The dimension of region I is 60×44 km^2 and that of region II is 27×22 km^2. The grid interval is 1 km in region I and 500m in region II.

3.3. Results of the Oshima-Island model

The response of Oshima Island (transfer function) was calculated by averaging the system functions at 65 shoreline grid points over each frequency band. As shown in Fig. 14, the dependence on the incident direction can be found owing to asymmetry of bottom topography and shape of the island, but the averaged transfer function indicates three characteristic peaks at about 6.4 (0.16 c.p.m.), 5.0 (0.20 c.p.m.) and 4.0 minutes (0.25 c.p.m.). The amplification factor ranges from 5 to 7 at periods shorter than 6 min. Especially, in the case of input from south or west, a remarkable peak can be seen at approximately 8.0 min (0.13 c.p.m.).

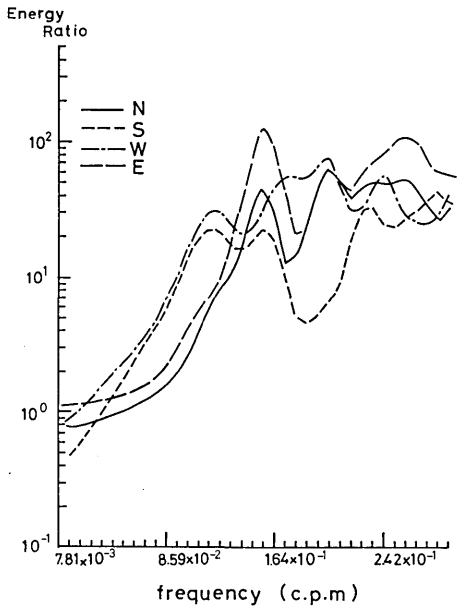

Fig. 14. Transfer function in the Oshima model for each direction of the incident wave. Transfer function is calculated by averaging the system functions at 65 shoreline grid points over each frequency band.

Relative energy with respect to the incident wave energy at the grid points of Senzu, Komatsubayashi, Sashikiji and Nomashi is illustrated in Fig. 15 as a function of frequency. Dependence on the incident angle is also seen here, but since in reality the external disturbances generally approach from the south or west, we had better take notice of these two directions.

There exist peaks at about 6 min and 4 min whose levels are higher at Sashikiji and Nomashi than at Senzu and Komatsubayashi. Further-

more, at Sashikiji and Nomashi, there exists another remarkable peak of about 8 minutes. At Nomashi a peak of 8.53 min with the amplification factor of 10.9 is found for southerly input, and a peak of 8.00 min with 14.6 times amplification is found for westerly input.

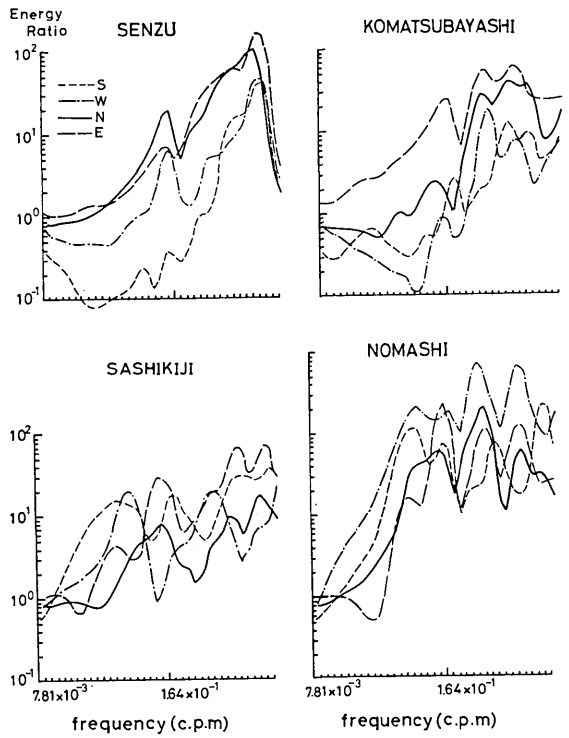

Fig. 15. Energy ratio to input spectrum at Senzu, Komatsubayashi, Sashikiji and Nomashi in the Oshima model.

It is emphasized that in the case of the input wave of approximately 8 min, the response on the western side of the island differs from that on the eastern side, and these results are qualitatively in accordance with the field observation. Therefore, we investigate the amplitude distribution around the island for continuous input of sine wave at this period.

Fig. 16 shows contours of sea level variations for southerly input with a period of 8.0 min after equilibrium. In this figure the solid lines and the broken lines indicate that they are not in phase with each other. Large amplitudes are seen in the western and southern region, showing the standing wave pattern which has a node in a southwesterly direction vis-a-vis the island. This oscillation pattern which appears in the Oshima

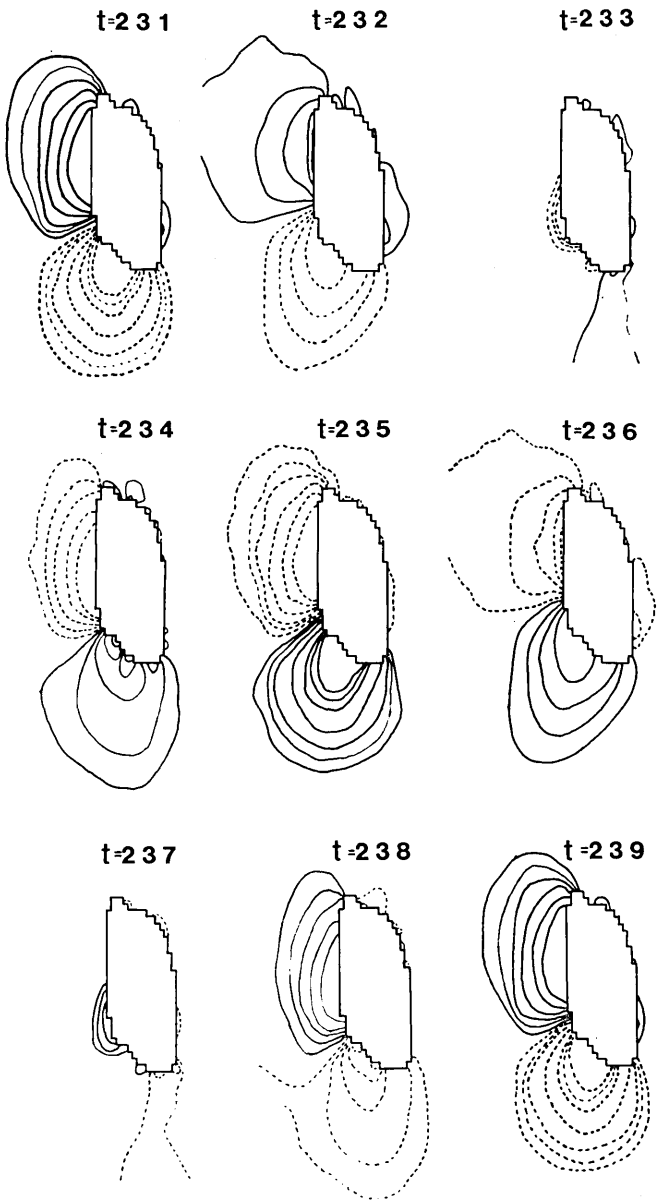

Fig. 16. Sequential patterns of the water level for the southerly input of a sine wave with a period of 8 min. Incident waves approach from the south (lower side of each figure) and t shows the time step in minutes from the start of the calculation. Solid lines and broken lines indicate that they are out of phase with each other.

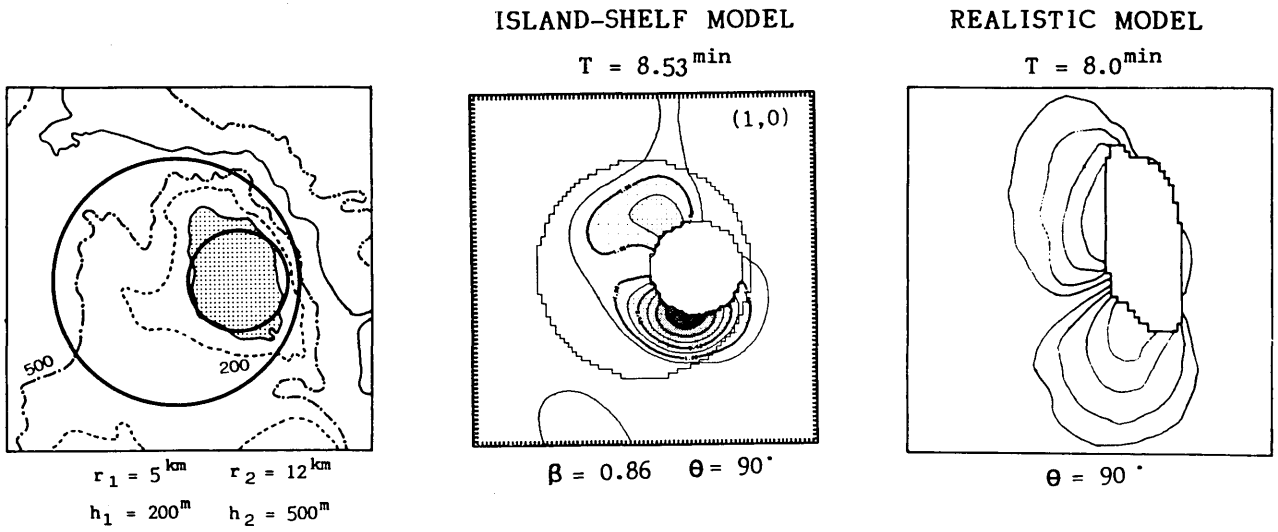

Fig. 17. Comparison of realistic Oshima model with the Island-Shelf model. Incident waves approach from the south (lower side of the figure). The distribution pattern of the Island-Shelf model indicates the modified (1, 0) mode.

model by giving realistic topography is similar to the result in the Island-Shelf model with parameters $\beta=0.8$, $\theta=90°$ as shown in Fig. 7-(b). That is to say, it is conceivable that this pattern shows the modified (1, 0) mode and large responses are limited by asymmetry in a zone with the broader shelf.

For trial, we replace realistic Oshima Island with a round island with a radius of 5 km surrounded by a circular sill with a radius of 12 km and a depth of 200m, beyond which water with a depth of 500m extends. We investigate in this simple model how the (1, 0) mode in the symmetric case is modified for southerly input (see Fig. 17). As shown in the figure, the result of the Island-Shelf model at a period of 8.53 min corresponds relatively well with that of the realistic model at a period of 8.00 min. Therefore we can identify the standing wave pattern of a period of 8.0 min as the (1, 0) mode modified by asymmetry of an insular shelf. This model does not contradict the observed fact that there exists an energy peak of approximately 8 min at Nomashi, and the energy level at Senzu and Komatsubayashi is much less than at Nomashi.

From the present study we can regard Oshima Island as a resonator, namely the incident wave of a period of about 8 min is amplified by about ten times at Nomashi. But it is to be emphasized that this response can be obtained under continuous forcing. As the asymmetry of the insular shelf becomes pronounced, we can presume intuitively the energy loss increases more than in the symmetric case. To obtain a rough idea of wave damping, we stopped the forcing with resonant frequency in the realistic Oshima model. Then it is seen that the amplitude damped to half after 3 wave cycles at Nomashi and Sashikiji and after 2 wave cycles at Senzu and Komatsubayashi which seem to be reasonable; the so-called quality factor Q is about 10 to 15.

4. Conclusions

We examined the effect of the asymmetric shape of an insular shelf in trapping long waves around an island.

4.1. Results of the Island-Shelf model

The Island-Shelf model used here is perhaps the most simple model (of many possible variations) which can represent asymmetry. In the present model, the conditions of wave trapping are considered to be controlled by the parameters as follows: (a) the ratio of radius (r_1/r_2), (b) the ratio of depths (h_1/h_2), (c) the relative distance between the center of the island and that of the sill ($\beta=\Delta r/(r_2-r_1)$), and (d) the incident direction (θ). Yet, these parameters are not independent of each other

in specifying the trapping conditions (and consequently determining the wave response around the island). In the present study we fixed the ratios r_1/r_2 and h_1/h_2, so that the results could be used as case studies. We found the following:

(1) As the asymmetry becomes pronounced, a large response region shifts to the direction of a broader shelf as a whole.

(2) We can surmise that the transfer function in the case of the asymmetric island can be estimated by using the solution of a symmetric island model whose width of the round shelf coincides with the broadest width of shelf in the asymmetric model.

Since the tendency of these results is also seen in the model which roughly approximates Oshima Island, these characteristics may be fundamental and not significantly influenced by r_1/r_2, h_1/h_2. Thus, there seems to exist a clear physical mechanism; a mechanism which we cannot explain as yet.

In this study we have traced the movement of spatial patterns which are based on the characteristic modes of the symmetric case. The reason for doing so is that we couldn't estimate in advance the resonant frequencies of an asymmetric case. Furthermore, even if we did fix a specific frequency, an infinite number of modes would be included. So we meet with difficulty in clarifying the contributions of various modes quantitatively. Even in lower modes, the characteristic frequencies and energy levels differ subtly for each mode and incident angle. Therefore, when higher modes overlap, we cannot make a generalization regarding the wave trapping phenomena around the asymmetric island as yet.

Moreover, it remains a fundamental question whether we can apply the idea of modes in the symmetric case in the same way when the asymmetry becomes pronounced. In other words, if the insular shelf is asymmetric, ray paths will exist which return in the same phase to their starting points without completing one or more circuits around the island. That is, on the one hand, some modes can exist only in the asymmetric case, while on the other hand, there can exist modes which cannot exist in the asymmetric case. Hence both the selection and the modification of symmetric modes will occur as a result of asymmetry. It is noteworthy that not only characteristic frequencies, but also energy levels can be roughly estimated by the method used in (2).

In the actual ocean environment, various asymmetries exist which cannot be expressed in the present model. For example, the shape of Oshima is more elliptical than circular, and the surrounding bottom topography is much more complicated. But even with a rough model (as shown in Fig. 17), the response pattern of the (1, 0) mode agrees fairly well with the results of the Oshima-Island model. This indicates that

the result of (2) is sufficient in estimating a transfer function in 0-th order approximation.

BERNARD (1976) made a similar study in that he compared a numerical solution with the analytical solution of an island with parabolic depth (HOMMA, 1950). In his model, a discrepancy occurred at high frequencies, and he proposed that the lowest predictable period is $4\Delta s/\sqrt{gh_{\min}}$ where Δs is grid size and $h_{\min}$ is the shallowest depth. This means that four grid points are necessary to describe a wave. We adopt the same scheme (as BERNARD) in our Island-Shelf model, but the results show that we need at least ten grid points to describe a wave.

4.2. Observational results around Oshima Island

There has hitherto been little observation of water levels around the island. LONGUET-HIGGINS (1967) once presumed that the observed waves around Macquarie Island correspond to the mode $n=7$. But those records were obtained at only one station and consequently the evidence was insufficient to draw any type of conclusion regarding the trapping waves around the island.

Present observation has revealed that (1) the power level is higher in the western or southern region where the shoal is spread, and (2) a characteristic spectrum peak at a period of approximately 8 min can be detected at Nomashi.

During the observations, the weather was fine under the atmospheric high pressure, and the sea was calm. Therefore, we may have been fortunate enough to observe responses in the wide frequency range. But considering the scale of Oshima Island, a sampling interval of 1 min adopted in the observation was too long to discuss the energy peaks of 6, 5 and 4 min found in the Oshima-Model.

We didn't discuss a phase lag of oscillations observed at various stations because the coherency was low at periods below 30 min. One reason may be attributed to the fact that the energy levels at Senzu and Komatsubayashi are low and their characteristic responses may be hidden in noise levels. Furthermore, it is possible that the fluctuations of these short periods are much affected by the local topography; perhaps being generated by nonlinear phenomena in the nearshore zone. However, the coast of Oshima Island is made up mainly of craggy cliffs and we can presume that phenomena such as surfbeats occur only infrequently.

4.3. Results of the Oshima model

Numerical experiments were carried out in the Oshima model (using the actual bathymetry) and in the Island-Shelf model (with the smoothed bottom topography around Oshima Island). It may be concluded that the

oscillation of a period of 8 min is a (1, 0) mode of edge wave modified by the asymmetry of the insular shelf and corresponds to the standing wave pattern with a node in a southwesterly direction vis-a-vis the island. These results are consistent qualitatively with the field observation. To confirm the validity of these results, we need to observe the water level at the point near a node which is predicted by the numerical model.

Acknowledgements

The author wishes to express his sincere gratitude to Prof. K. Kajiura for invaluable guidance in the course of this work. He also expresses his thanks to Assistant Prof. I. Aida for the advice received on numerical computation.

All the computations were made by utilizing the facilities of the computer center of the University of Tokyo.

References

AIDA, I., 1974, Numerical computation of a tsunami based on a fault origin model of an earthquake, *J. Seismol, Soc. Japan.*, Ser. II, **27**, 141-154 (in Japanese).

BARNARD, B. J. S., PRITCHARD, W. G. and PROVIS, D. G., 1983, Experiments on wave trapping by a submerged cylindrical island, *Geophys. Astrophys. Fluid Dynamics*, **24**, 23-48.

BERNARD, E. N., 1976, A numerical study of the tsunami response of the Hawaian Islands, *H. I. G.*, 76-6.

HASHIMOTO, M., AIDA, I., SAKASHITA, S. and KOYAMA, M., 1986, On the characteristics of long-period fluctuations of the water level observed around Oshima Island, *Bull. Earthq. Res. Inst., Univ. Tokyo*, **61**, 129-142 (in Japanese).

HOMMA, S., 1950. On the behavior of seismic sea waves around a circular island, *Geophys. Mag.*, **21**, 199-208.

LONGUET-HIGGINS, M. S., 1967, On the trapping of wave energy round islands, *J. Fluid. Mech.*, **29**, 781-821.

RENARDY, Y., 1983, Trapping of water waves above a round sill, *J. Fluid. Mech.*, **132**, 105-118.

SUMMERFIELD, W., 1972, Circular islands as resonators of long-wave energy, *Philos. Trans. R. Soc. London*, Ser. A, **272**, 361-402.

Appendix; Analytic transfer function for a symmetric island

Consider a steep-sided round island of radius r_1 surrounded by a circular sill of radius r_2 and depth h_1, beyond which deep water of depth $h_2>h_1$ extends. For simple harmonic waves with frequency ω, the wave-number is $k_1=\omega/\sqrt{gh_1}$ in the region above the sill $r<r_2$ and $k_2=\omega/\sqrt{gh_2}$ outside of the sill $r>r_2$.

Let the incident wave approach from $x\sim-\infty$ with unit amplitude so that

$$\eta^I=e^{i(k_2x-\omega t)}=e^{i(k_2r\cdot\cos\theta-\omega t)} \tag{A. 1}$$

In the region $r>r_2$, there must be scattered waves η^R which propagate away to $r\sim\infty$.

Let us consider

$$\eta_2=\eta^I+\eta^R \tag{A. 2}$$

and for integer n

$$\eta^R=\zeta^R(r)\cdot e^{i(n\theta-\omega t)}. \tag{A. 3}$$

So that ζ^R satisfies in polar coordinates,

$$\nabla^2\zeta^R+k_2^2\zeta^R=0 \tag{A. 4}$$

and must vanish as $r\to\infty$.

Consider similarly above the sill $r<r_2$

$$\eta_1=\zeta_1(r)\cdot e^{i(n\theta-\omega t)}. \tag{A. 5}$$

The displacement satisfies

$$\nabla^2\zeta_1+k_1^2\zeta_1=0. \tag{A. 6}$$

Boundary conditions at the edge of sill and the coast are

$$\begin{cases} \zeta_1=\zeta_2 & \text{at} \quad r=r_2 \\ h_1\dfrac{\partial\zeta_1}{\partial r}=h_2\dfrac{\partial\zeta_2}{\partial r} & \text{at} \quad r=r_2 \\ \dfrac{\partial\zeta_1}{\partial r}=0 & \text{at} \quad r=r_1. \end{cases} \tag{A. 7}$$

The incident plane wave η^I can be expanded as follows.

$$\eta^I=\sum_{n=-\infty}^{\infty}\frac{1}{2}i^n\cdot[H_n^{(1)}(k_2r)+H_n^{(2)}(k_2r)]\cdot\exp\{i(n\theta-\omega t)\}. \tag{A. 8}$$

So that we propose the following solution for η.

$$\eta(r,\theta,t)=\sum_{n=-\infty}^{\infty}\exp\{i(n\theta-\omega t)\}\cdot\begin{cases} A_nH_n^{(1)}(k_1r)+B_nH_n^{(2)}(k_1r) & (0<r_1<r<r_2) \\ \left(C_n+\dfrac{1}{2}i^n\right)H_n^{(1)}(k_2r)+\dfrac{1}{2}i^nH_n^{(2)}(k_2r) & (r>r_2) \end{cases} \tag{A. 9}$$

where

$$A_n=\frac{2i^{n+1}H_n^{(2)'}(\alpha\nu)}{\pi\varepsilon\nu\, E(\nu;\varepsilon,\alpha,n)},\qquad B_n=\frac{-2i^{n+1}H_n^{(1)'}(\alpha\nu)}{\pi\varepsilon\nu\, E(\nu;\varepsilon,\alpha,n)},$$

$$C_n+\frac{1}{2}i^n=(-1)\left(\frac{1}{2}\right)i^n\frac{E_s(\nu;\varepsilon,\alpha,n)}{E(\nu;\varepsilon,\alpha,n)}$$

$$\begin{aligned}E(\nu;\varepsilon,\alpha,n)=&\varepsilon H_n^{(1)}(\varepsilon\nu)\cdot[H_n^{(1)'}(\alpha\nu)H_n^{(2)'}(\nu)-H_n^{(2)'}(\alpha\nu)H_n^{(1)'}(\nu)]\\&-H_n^{(1)'}(\varepsilon\nu)\cdot[H_n^{(1)'}(\alpha\nu)H_n^{(2)}(\nu)-H_n^{(2)'}(\alpha\nu)H_n^{(1)}(\nu)]\\E_s(\nu;\varepsilon,\alpha,n)=&\varepsilon H_n^{(2)}(\varepsilon\nu)\cdot[H_n^{(1)'}(\alpha\nu)H_n^{(2)'}(\nu)-H_n^{(2)'}(\alpha\nu)H_n^{(1)'}(\nu)]\\&-H_n^{(2)'}(\varepsilon\nu)\cdot[H_n^{(1)'}(\alpha\nu)H_n^{(2)}(\nu)-H_n^{(2)'}(\alpha\nu)H_n^{(1)}(\nu)]\end{aligned}$$

$$\nu=k_1r_2,\quad \varepsilon=(h_1/h_2)^{1/2},\quad \alpha=r_1/r_2.$$

$H_n^{(1),(2)}$; n-th order Hankel function of the first (second) kind and primes denote derivations with respect to the argument.

The disturbance in water level at the coast is found by setting $r=r_1$ in the appropriate part of (A. 9), so we can obtain the analytical transfer function as follows.

$$\overline{\eta(r_1,\theta,t)^2}=\frac{36}{\pi^4\varepsilon^2\alpha^2\nu^4}\cdot\sum_{n=0}^{\infty}\left|\frac{\varepsilon_n i^n}{E(\nu;\varepsilon,\alpha,n)}\right|^2 \tag{A. 10}$$

where the average is with respect to θ over the range 0 to 2π, and

$$\varepsilon_n=\begin{cases}1 & n=0\\ 2 & n\neq 0\end{cases}$$

The terms $|\varepsilon_n i^n/E(\nu;\varepsilon,\alpha,n)|^2$ converge rapidly, and we summed up to $n=13$ in the present study.

島棚の非対称性が長波の捕捉に及ぼす影響

地震研究所　橋　本　道　明*

島棚の非対称性が重力長波の捕捉に及ぼす影響について数値実験を行った．円形の島の中心が円形の棚の中心から Δr 離れている Island-Shelf model を使用して，棚巾の非対称性を表現した．その結果，(1) 非対称性が強まると，高振幅領域は概ね広がった棚の方向に移行する，(2) 非対称時の伝達関数は，最も広い棚巾を新たな棚巾とした対称時の解析解で代用しうることが示された．

伊豆大島の周囲4点で水位の同時観測を行ったところ，浅瀬の広がった島の西側の測点で周期8分前後の特徴的なスペクトルピークが認められた．この特性を理解するため，現実の水深を与えた大島モデル，大島近海を粗く近似した Island-Shelf model による数値計算を行った．その結果，この周期の振動は (1, 0) モードのエッジ波に対応している可能性が示された．このモードは島棚の非対称性により変形され，島の南西方向に節を持つ定在振動パターンを形成している．

* 現在 (財) 日本気象協会